PACE OCI Polarization Sensitivity Based on Pre-launch Testing

Jeff McIntire[a], Eugene Waluschka[b], Gerhard Meister[c], Joseph Knuble[c], and William B. Cook[c]

[a]Science Systems and Applications Inc, Lanham, MD 20706 USA
[b]Stellar Solutions, Palo Alto, CA 94306 USA
[c]NASA Goddard Space Flight Center, Greenbelt, MD, 20771 USA

ABSTRACT

The Ocean Color Instrument (OCI) is a sensor on the upcoming Plankton, Aerosol, Cloud, ocean Ecosystem (PACE) mission, scheduled for launch in early 2024. OCI is a grating spectrometer with hyperspectral coverage from the ultraviolet (about 310 nm) to near-infrared (about 900 nm), with additional filtered channels in the short-wave infrared (940 nm – 2260 nm). This instrument will provide ocean color science data to continue the data sets collected by heritage sensors MODIS, SeaWiFs, and VIIRS, but with increased spectral coverage and improved accuracy. In order to achieve the high levels of accuracy demanded by the science community, a rigorous ground test program was conducted to calibrate the instrument and ensure that the calibration can be transferred to on-orbit operations. Some calibration parameters can only be measured during pre-launch testing; one such parameter is the polarization sensitivity. Polarization testing measured the Mueller matrix components needed to determine the polarization sensitivity for all spectral bands for a series of telescope scan angles covering the expected on-orbit scan range. Results indicate that the sensitivity is below 0.6 % except at the shortest wavelengths (less than 340 nm) and was characterized to better than 0.1 % above 340 nm. This indicates that any polarized scenes measured on orbit can be corrected for with a high degree of confidence.

Keywords: PACE, OCI, polarization, calibration

1. INTRODUCTION

The Plankton Aerosol Cloud ocean Ecosystem (PACE) satellite is a next generation platform for on-orbit remote sensing of ocean science, with a payload to include the Ocean Color Instrument (OCI) and a pair of polarimeters (SPEXone and HARP2).[1–3] At the time of writing, all three instruments have undergone comprehensive pre-launch characterization and performance assessments, have been integrated onto the spacecraft, and are scheduled for launch in early 2024. Although the OCI design is partly based on heritage sensors MODIS, VIIRS, and SeaWiFS[4,5] which were widely used for ocean research, there have been a number of design improvements. OCI is a grating spectrometer with hyperspectral coverage from about 310 nm to 900 nm with 9 additional filtered channels in the SWIR spectral region (for reference, earlier sensors were filtered radiometers). OCI completed its pre-launch characterization including comparison to design requirements (intended to ensure high quality performance once on orbit) and characterization of performance metrics necessary to transfer the calibration to on-orbit operations. One parameter that must be measured prior to launch is the polarization sensitivity. On-orbit scenes can be highly polarized due to Rayleigh scattering or Sun glint, so measurements of a sensor's sensitivity to linearly polarized light (or linear diattenuation) are essential to correct the science data and maintain accuracy for the science community. This paper will describe the measurements and results of the pre-launch characterization of the linear diattenuation for the OCI Flight unit; similar results for the OCI engineering unit were described in.[6] Section 2 will briefly describe the OCI instrument and the test setup; Section 3 will provide an overview of the analysis methodology; and Section 4 will review the analysis results and sensor comparison followed by conclusions in Section 5.

Send correspondence to Jeff McIntire: jeffrey.mcintire@ssaihq.com

2. OVERVIEW

2.1 OCI Overview

OCI has a rotating telescope that consists of a primary mirror, a depolarizer, and a secondary mirror that spins at roughly 6 Hz in a plane perpendicular to the direction of the spacecraft motion,[1–3] similar to heritage sensors such as VIIRS and SeaWiFS.[4,5] The telescope scans a swath of the Earth covering $\pm$ 56 degrees off nadir as well as a dark view at roughly 180 degrees off nadir and a solar calibration view at about -90 degrees off nadir (which will be used to calibrate the instrument once on orbit). The light, after it passes through the rotating telescope is directed onto a Half Angle Mirror (HAM), rotating at half the speed of the telescope, that de-rotates the light beam which then illuminates a slit oriented such that the slit image on the ground is also perpendicular to the direction of spacecraft motion. The light next passes through a weak field lens and is then reflected off an off-axis parabolic mirror which collimates the light. A dichroic beamsplitter separates out wavelengths below about 600 nm and directs them through a clear aperture onto a grating which separates the light and focuses it (through a lenslet array) onto a CCD detector. Wavelengths above 600 nm pass through the first dichroic and encounter a second dichroic beamsplitter that separates out roughly 600 nm to 900 nm and directs that light through a clear aperture onto a second grating which separates the light and focuses it (through a lenslet array) onto a second CCD detector. Longer wavelengths pass through the second dichroic, are reflected off a collimating mirror into a micro lens array, and then through a series of fibers that terminate in the short-wave infrared (SWIR) detector assembly. There are 16 fibers, each of which terminates at a dichroic that separates the light and directs the two beams through bandpass filters to either InGaAs or HgCdTe detectors, which are aggregated into 9 separate SWIR bands.

Each of the two CCD detectors is a 128 x 512 array of physical pixels. The gratings separate the light in the direction of the larger dimension (512, or the spectral dimension) and the image across the smaller dimension (128, or the spatial dimension) corresponds to the long axis of the slit. The short axis of the slit corresponds to about 8 pixels in the spectral direction. As an image on the ground comes into view on the leading edge of the long axis of the slit, it is imaged onto the CCD. As the image moves across the slit, and consequently across the CCD in the spatial dimension, it is recorded again multiple times, which is summed via time delay integration (TDI). Each CCD has the option of variable aggregation of 1, 2, 4, or 8 pixels in either spectral and spatial directions. The baseline science pixel is an 8 x 8 aggregation (spatial versus spectral) of physical pixels; however, there are instrument modes intended for on-orbit use that utilize smaller aggregation schemes (such as solar or lunar calibration). The analysis performed in this work uses data aggregated into 8 x 1, or aggregated in the spatial direction but with the full spectral resolution.

The OCI instrument has a number of design requirements intended to ensure that once on orbit, OCI data is of sufficient accuracy to produce high quality science products and trend them over the mission lifetime. For polarization, there are two requirements. The first requirement limits the maximum linear diattenuation to 1 % for the hyperspectral bands above 345 nm and 2 % for the SWIR bands. The second requirement places an upper bound on the total uncertainty to 0.17 % from 345 nm to 400 nm and 0.11 % above 400 nm for the hyperspectral bands (there is no specified uncertainty limit for the SWIR bands). The assessment of OCI's performance versus the first requirement will be detailed in the results discussion (Section 4); a discussion of the uncertainty requirement is left for future work.

2.2 Testing Overview

OCI was integrated and tested at the NASA Goddard Space Flight Center in Greenbelt, MD from late 2021 to late 2022, including both ambient and environmental testing. The polarization testing was performed twice over the course of the test program: once in ambient early in testing and once near the end of testing in thermal vacuum. For each test, a 20 inch integrating sphere was illuminated by a 250 W halogen lamp (to cover the VIS, NIR, and SWIR) and a laser-driven light source (to cover the UV and VIS). The light exited the sphere through a 8 inch circular aperture. The light then passes through a MOXTEK® wire grid polarizer mounted in a rotary stage. During testing, the rotary stage is cycled through 720 degrees rotation in 15 degree increments. Baffling is in place to ensure light only passes through the polarizer aperture. The polarizer was tilted 5 degrees in the horizontal direction to ensure any reflections off OCI back to the polarizer would no longer be in the path.

For the ambient test, OCI was placed on a rotating table with the scan plane perpendicular to gravity.[3,7] During this test, the table was rotated such that OCI viewed the integrating sphere at 5 scan angles: ± 49 degrees, ± 25 degrees, and 0 degrees (measured twice as a check on repeatability). In the nominal configuration, the solar calibration port on OCI is obstructed by the table, so OCI was repositioned on the table and two additional measurements were taken at -90 degrees and -52 degrees. Note that at this stage in testing, the solar calibration assembly had not yet been installed, so the telescope could be viewed directly through the solar calibration port. At the beginning of the test, an additional polarizer with the transmission axis fixed was inserted into the path between the rotating polarizer and OCI; this allowed the efficiency of the polarizer to be measured by OCI (this efficiency measurement will be discussed in a future work). In thermal vacuum, OCI was placed inside the vacuum chamber and viewed the sphere through the chamber window; here data was only taken at nadir. In ambient, the SWIR bands 1615 nm, 2230 nm, and 2260 nm could not be cooled (these bands use HgCdTe detectors that do not produce meaningful results unless cooled); in thermal vaccum, these detectors were cooled.

3. METHODOLOGY

The OCI polarization sensitvity measurements were analyzed using a Fourier analysis. The offset corrected digital counts (dn) for a given polarizer angle θ were modeled as a fourth order Fourier expansion, or[8]

$$dn\left(\theta\right) = \frac{1}{2}c_0 + \sum_{n=1}^{4} c_n \sin\left(n\theta\right) + d_n \cos\left(n\theta\right) \tag{1}$$

where the coefficients are given by

$$\frac{1}{2}c_0 = \frac{1}{\pi}\int_0^{2\pi} dn\left(\theta\right) d\theta \tag{2}$$

$$C_n = \frac{2c_n}{c_0} = \frac{2}{\pi c_0}\int_0^{2\pi} dn\left(\theta\right)\cos\left(n\theta\right) d\theta \tag{3}$$

$$D_n = \frac{2d_n}{c_0} = \frac{2}{\pi c_0}\int_0^{2\pi} dn\left(\theta\right)\sin\left(n\theta\right) d\theta \tag{4}$$

Here the coefficients C_2 and D_2 are the Mueller matrix components m_{12} and m_{13}.[9] The Fourier expansion given in Eq. (1) can be rewritten as

$$dn\left(\theta\right) = \frac{1}{2}c_0\left(\lambda\right)\left[1 + \sum_{n=1}^{4} a_n \cos\left(n\theta + 2\delta_n\right)\right] \tag{5}$$

where the amplitude of the polarization is given by

$$a_n = \frac{\sqrt{C_n^2 + D_n^2}}{\sqrt{a_2^{eff}}} \tag{6}$$

where a_2^{eff} is the polarizer efficiency determined from Eq. (6) without the denominator using the data from testing in which the additional fixed polarizer was inserted in the path. Note that a_2 is the linear diattenuation (LD). The phase angle is determined from

$$\delta_n = \frac{1}{2}\arctan\left[\frac{D_n}{C_n}\right] \tag{7}$$

A full uncertainty analysis was also performed; the discussion of the uncertainties is left for future work.

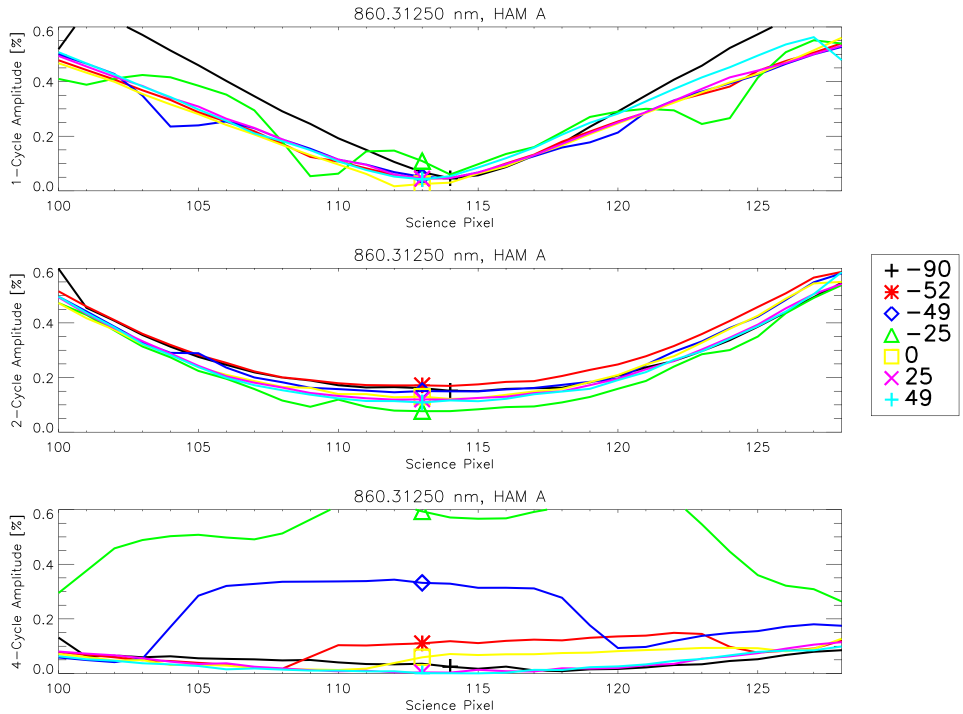

Figure 1. 1, 2, and 4-cycle Fourier amplitudes plotted versus pixel as OCI scans across the integrating sphere aperture (upper, middle, and lower plots). The legend denotes the colors / symbols corresponding to different OCI scan angles.

4. ANALYSIS RESULTS

4.1 Data Quality and Reduction

As OCI scanned across the integrating sphere, there is a scan angle range for which the OCI footprint was fully inside the sphere aperture (about 3 degrees). Thirty-five seconds of data were taken at each polarizer angle in the sequence. Each recorded pixel was averaged over all valid scans in each data collection (HAM sides being treated separately). The dark offset data (collected at 180 degrees off nadir inside the instrument) was also recorded every scan, and averaged over scans. The offset corrected signal (dn) is then the scan averaged signal minus the scan averaged dark offset for every pixel. Outlier rejection was performed at every step. This process was repeated for all scan angles listed in Section 2.2. The Fourier analysis described in Section 3 was performed for every pixel for which the OCI footprint was within the integrating sphere aperture.

4.2 Results

The Fourier amplitudes as a function of pixel as OCI scans across the integrating sphere aperture are plotted in Figure 1. Here the 1, 2, and 4-cycle amplitudes are shown in the upper, middle, and lower subplots. The results derived at the different scan angles measured are overlaid using colors defined in the legend. In the upper plot, the 1-cycle amplitude is V-shaped as a function of pixel, with a minimum where the OCI view angle is at the center of the polarizer. This is expected when there is a linear transmission gradient in the polarizer.[6] To minimize 1-cycle contamination in the analysis, the most common minimum pixel over all bands is used in subsequent analysis (analyzed per scan angle and denoted by the symbols in all three plots). The 2-cycle amplitudes shown in the middle plot also show some dependence on pixel location. The lowest plot graphs the 4-cycle amplitudes as a function of pixel. Note that the 4-cycle amplitudes dominate the measurements at -25

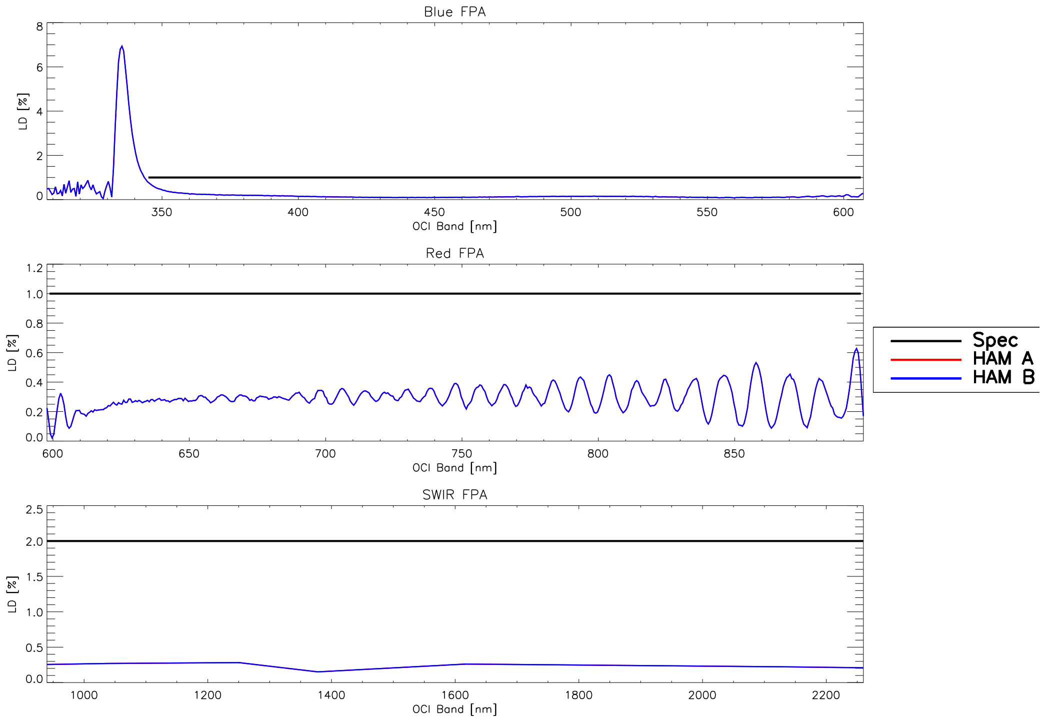

Figure 2. Linear diattenuation (LD) plotted for each FPA using thermal vacuum data (in %). Results from HAM sides A and B denoted by red and blue lines. The OCI design requirement is shown by the black line.

degrees scan angle, and are significant at -49 degrees scan angle. Possibilities include stray light contamination or retro-reflections off the polarizer / back of the sphere. For the -25 degree measurements, the 2-cycle amplitudes seem to be out-of-family as a function of scan angle; these results will not be used in the on-orbit correction tables.

The measured linear diattenuation (LD) are plotted in Figure 2 at nadir for both HAM sides (red and blue lines). The upper plot shows the amplitudes for the blue FPA; the middle plot graphs the amplitudes for the red FPA; and the lower plot shows the amplitudes for the SWIR bands. These results were derived from environmental testing. The sensor design requirement limits the LD to 1.0 % for all bands on the blue and red FPAs above 345 nm and 2 % on the SWIR FPA, as shown by a solid black line in the plots. All OCI bands subjected to the requirement were well beneath this limit; the amplitude is below ∼0.6 % above 345 nm. Note that the diattenuation begins to rise sharply below 340 nm. There is a spectral region from 330 nm to 340 nm for which the diattenuation can reach almost 7 %. Below 330 nm, the test signal was very low, well below the calculated uncertainties (as a result, this data is excluded from the on-orbit correction tables). Also of interest is the oscillations in the diattenuation that occur in the red FPA; these oscillations in wavelength are caused by the dependence on optical path as a function of thickness and refractive indices of the double wedge.[10] Some wavelengths see a predominately full waveplate behavior (no change in polarization), others see a predominately half-waveplate behavior (90 degree rotation), and most see something in between. As a result, the net polarization at some wavelengths will weight towards transmission while other wavelengths will weight towards rejection. This manifests as a sinusoidal oscillation versus wavelength. Also, note that the HAM side dependence is very small.

The measurements for the linear diattenuation for the range of scan angles measured is plotted in Figure 3 for HAM side A. Again, the results for the blue, red, and SWIR FPAs are shown in the upper, middle, and

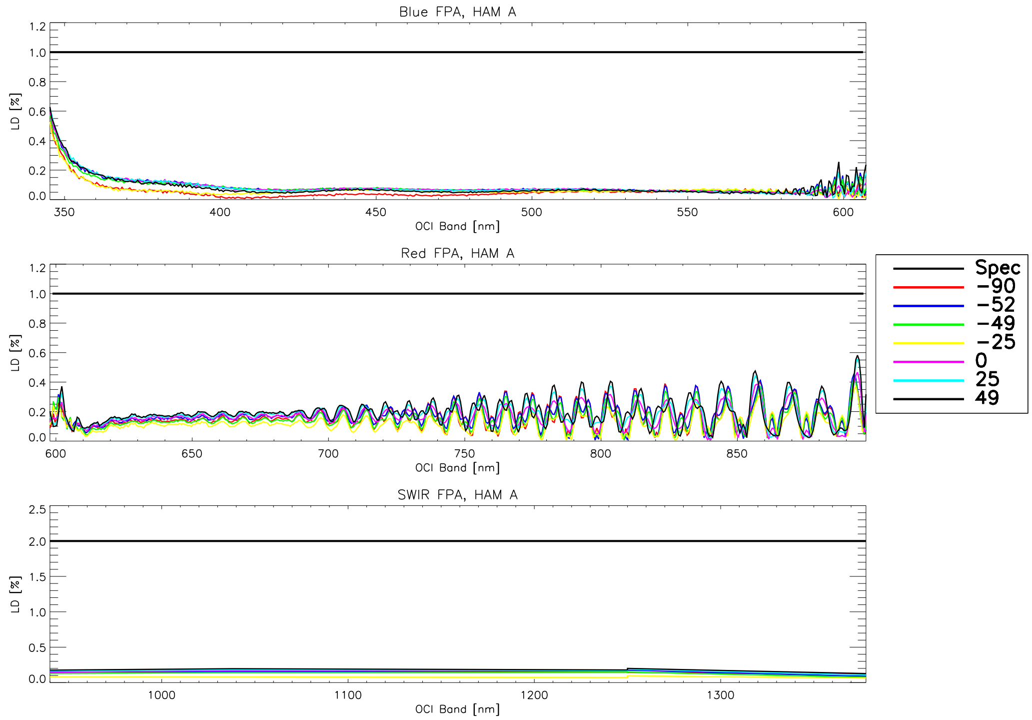

Figure 3. Linear diattenuation (LD) plotted for each FPA using ambient data (in %). Results from different scan angles are denoted by the colored lines defined in the legend. The OCI design requirement is shown by the black line.

lower plots. Here the blue FPA plot is limited to bands above 345 nm to reduce the scale. The plots show limited variation with scan angle. The main features are consistent over most scan angles. The measurements for -25 degrees scan angle are out-of-family, due to the large 4-cycle variations observed for this data set (shown in Figure 1). While in principle, the 2 and 4-cycle components of a Fourier series are orthogonal; in practice, the added variation makes the 2-cycle determination more difficult. As a result, the final data set used to create the on-orbit correction for OCI does not include these measurements. The SWIR FPA plot only includes bands up to 1378 nm as the bands above this were only measured in thermal vacuum at a single scan angle (nadir).

Overall, the OCI Flight measurements of the polarization sensitivity were very successful. The magnitude of the linear diattenuation was well within the sensor design requirements for all bands. In addition, the linear diattenuation and phase angle were well characterized for all bands as well as across scan angles. The uncertainties on the measurement (to be discussed in a future work) were also well within expectations. The results shown here form the basis of the tables that will be used to correct OCI data once on orbit.

5. CONCLUSIONS

The OCI instrument onboard the upcoming PACE mission has undergone a rigorous and comprehensive pre-launch test campaign and is scheduled to launch in early 2024. The test campaign measured a number of parameters necessary to transfer the calibration to on-orbit operations and ensure high quality science data once on orbit.[11] One parameter of interest is the sensitivity to linear polarized light, or linear diattenuation. The measured diattenuation was well within the design requirements for OCI and was elow 0.6 % for all bands above 345 nm. In addition the uncertainties on the polarization sensitivity were well below expectations. This indicates that polarized scenes encountered on orbit can be corrected for with a high degree of confidence, ensuring the science team receives high quality data products from the PACE mission.

ACKNOWLEDGMENTS

The authors would like to acknowledge the following: the OCI test team for conducting the test and the science working group for useful comments on the analysis. The above mentioned provided valuable information and support to the analysis presented in this work.

REFERENCES

[1] Werdell, P., Behrenfeld, M., Bontempi, P., Boss, E., Cairns, B., Davis, G., Franz, B., Gliese, U., Gorman, E., Hasekamp, O., Knobelspiesse, K., Mannino, A., Martins, V., Mcclain, C., Meister, G., and Remer, L., "The plankton, aerosol, cloud, ocean ecosystem (PACE) mission: Status, science, advances," *Bulletin of the American Meteorological Society* **100**, 1775–1794 (2019).

[2] Gorman, E. T., Kubalak, D. A., Patel, D., Dress, A., Mott, D. B., Meister, G., and Werdell, P. J., "The NASA plankton, aerosol, cloud, ocean ecosystem (PACE) mission: an emerging era of global, hyperspectral earth system remote sensing," *Proc. SPIE* **11151**, 111510G (2019).

[3] Meister, G., Knuble, J. J., Chemerys, L. H., Choi, H., Collins, N. R., Eplee, R. E., Gliese, U., Gorman, E. T., Jepsen, K., Kitchen-Mckinley, S., Lee, S., McIntire, J. W., Patt, F. S., Tse, B. C., Waluschka, E., and Werdell, P. J., "Test results from the prelaunch characterization campaign of the engineering test unit of the ocean color instrument of NASA's Plankton, Aerosol, Cloud and Ocean Ecosystem mission," *Frontiers in Remote Sensing* , 59 (2022).

[4] Xiong, X., Butler, J., Chiang, K., Efremova, B., Lei, N., McIntire, J., Oudrari, H., Wang, Z., and Wu, A., "VIIRS on-orbit calibration methodology and performance," *Remote Sens.* **8**(1), 84 (2016).

[5] McClain, C. R., Feldman, G. C., and Hooker, S. B., "An overview of the SeaWiFS project and strategies for producing a climate research quality global ocean bio-optical time series," *Deep Sea Research Part II: Topical Studies in Oceanography* **51**(1) (2004).

[6] Waluschka, E., Collins, N. R., Cook, W. B., Gorman, E. T., Hilton, G. M., Knuble, J. J., Meister, G., and McIntire, J. W., "PACE ocean color instrument polarization testing and results," in [*Earth Observing Systems XXVI*], **11829**, 201–213, SPIE (2021).

[7] Knuble, J. J., Meister, G., Chemerys, L. H., Choi, H., Collins, N. R., Eplee, R. E., Gliese, U., Gorman, E. T., Jepsen, K., Kitchen-McKinley, S., Lee, S., McIntire, J. W., Patt, F. S., Tse, B. C., Waluschka, E., Field, C., McAndrew, B., Barsi, J., Sushkov, A., Bousquet, R., Cook, W., Werdell, P. J., McCarthy, J., Sharmin, M. S., and Hilton, G., "Pre-launch calibration methods of OCI on the PACE mission," *IGARSS* (2023). In press.

[8] McIntire, J., Moyer, D., Brown, S. W., Lykke, K. R., Waluschka, E., Oudrari, H., and Xiong, X., "Monochromatic measurements of the JPSS-1 VIIRS polarization sensitivity," *Applied optics* **55**(27), 7444–7454 (2016).

[9] Meister, G., Kwiatkowska, E. J., Franz, B. A., Patt, F. S., Feldman, G. C., and McClain, C. R., "Moderate-resolution imaging spectroradiometer ocean color polarization correction," *Applied Optics* **44**(26), 5524–5535 (2005).

[10] Waluschka, E., Wilson, M., Quijada, M., McAndrew, B., and Ding, L., "ORCA's depolarizer," in [*Earth Observing Systems XVI*], **8153**, 310–320, SPIE (2011).

[11] Meister, G., Knuble, J. J., Barsi, J., Bousquet, R., Chemerys, L. H., Choi, H., Collins, N. R., Eplee, R. E., Field, C. T., Gliese, U., Gorman, E. T., Hedelius, J. K., Jepsen, K., Kitchen-McKinley, S., Lee, S., McAndrew, B., McIntire, J. W., Patt, F. S., Squire, K. J., Sushkov, A., Tse, B. C., Waluschka, E., and Werdell, P. J., "Initial look at the results from the prelaunch characterization campaign of OCI on the PACE mission," *IGARSS* (2023). In press.